ACS APPLIED MATERIALS & INTERFACES

www.acsami.org

Research Article

Highly Stable Two-Dimensional Iron Monocarbide with Planar Hypercoordinate Moiety and Superior Li-Ion Storage Performance

Dong Fan, Chengke Chen, Shaohua Lu, Xiao Li, Meiyan Jiang, and Xiaojun Hu*

Cite This: *ACS Appl. Mater. Interfaces* 2020, 12, 30297−30303

Read Online

ACCESS | Metrics & More | Article Recommendations | Supporting Information

ABSTRACT: Stable planar hypercoordinate motifs have been recently demonstrated in two-dimensional (2D) confinement systems, while perfectly planar hypercoordinate motifs in 2D carbon−transition metal systems are rarely reported. Here, by using comprehensive *ab initio* computations, we discover two new iron monocarbide (FeC) binary sheets stabilized at 2D confined space, labeled as tetragonal-FeC (t-FeC) and orthorhombic-FeC (o-FeC), which are energetically more favorable compared with the previously reported square and honeycomb lattices. The proposed t-FeC is the global minimum configuration in the 2D space, and each carbon atom is four-coordinated with four ambient iron atoms, considered as the quasi-planar tetragonal lattice. Strikingly, the o-FeC monolayer is an orthorhombic phase with a perfectly planar pentacoordinate carbon moiety and a planar seven-coordinate iron moiety. These monolayers are the first example of a simultaneously pentacoordinate carbon and planar seven-coordinate Fe-containing material. State-of-the-art theoretical calculations confirm that all these monolayers have significantly dynamic, mechanical, and thermal stabilities. Among these two monolayers, the t-FeC monolayer shows a higher theoretical capacity (395 mAh g^{-1}) and can stably adsorb Li up to t-$FeCLi_4$ (1579 mAh g^{-1}). The low migration energy barrier is predicted as small as 0.26 eV for Li, which results in the fast diffusion of Li atoms on this monolayer, making it a promising candidate for lithium-ion battery material.

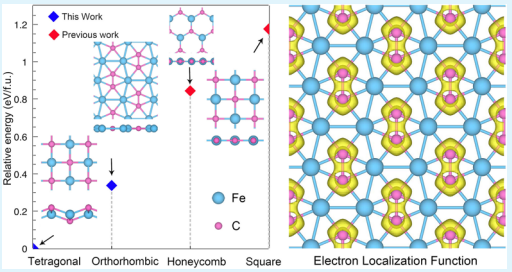

KEYWORDS: *planar hypercoordinate chemistry, chemical bond, first-principles calculation, two-dimensional material, Li-ion battery*

INTRODUCTION

Unconventional molecules with anomalous moieties and exotic electronic properties enrich nonclassical chemical bonding geometries and offer various potential applications because of due to their extraordinary electronic, chemical, and optical properties.[1,2] As an amazing and versatile element, carbon has typically sp^3-hybridized (i.e., diamond), sp^2-hybridized (i.e., graphene[3]), or linear sp-hybridized (i.e., carbyne[4]) bonding networks. Since the planar tetracoordinate carbon (ptC) has been first proposed by Hoffman et al. (1970)[5] and later synthesized in metal compound molecules (1977),[6] numerous stable ptCs molecules have been demonstrated theoretically and experimentally, such as (2,6-dimethoxyphenyl)lithium,[7] C−B−H systems,[8] C−Al systems,[9] and B−C systems.[10,11] Moreover, molecules containing planar carbon with even higher coordination have also been reported; i.e., Wang et al. theoretically predicted numerous minima molecules with planar hexa-, hepta-, and pentacoordinate carbons in B−C systems.[12] Aromatic boron wheels with a hypercoordinate carbon atom in C_2B_8, $C_3B_9^{3+}$, and $C_5B_{11}^{+}$ molecules were proposed by Erhardt et al.[13] Ito et al. reported a planar hexacoordinate carbon molecule, CB_6^{2-}, can be annulated by inserting arenes or olefins into a perimeter B−B bond.[14] It is also interesting to extend the planar hypercoordinate moieties to two-dimensional (2D) systems. Recently, some stable planar hypercoordinate motifs have been demonstrated in the 2D confinement systems: i.e., the B_2C graphene structure containing the ptC moiety and planar Be_2C monolayer with quasi-planar hexacoordinate carbons atoms were proposed by Wu et al. and Li et al., respectively.[15,16] Zhu et al. proposed eight transition-metal carbide monolayers with a planar pentacoordinate carbon moiety.[17] Yang et al. reported a Cu_2Si monolayer featuring planar hexacoordinate silicon and planar hexacoordinate copper,[18] and this monolayer has been synthesized very recently.[19]

However, there is rare literature precedents to date about perfectly planar hypercoordinate motifs in the 2D carbon−transition metal systems. The reported typical carbon−transition metal system, 2D Fe-based structure, is the freestanding monatomic suspended Fe membranes in graphene pores.[20] Inspired by this experimental observation, Thomsen et al. compared the stability of square and triangular lattice configurations for Fe embedded in graphene, Fe, and monatomic Fe carbide, suggesting that the square lattice was the most stable configuration.[21] Shao et al. also studied the

Received: February 27, 2020
Accepted: May 12, 2020
Published: May 12, 2020

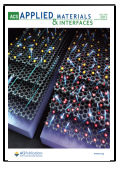

https://dx.doi.org/10.1021/acsami.0c03764
ACS Appl. Mater. Interfaces 2020, 12, 30297−30303

structural and electronic properties of Fe square lattices embedded in graphene pores, indicating that the distorted-square Fe_2C_2 lattice has the lowest energy.[22]

Herein, by means of *ab initio* computations, we designed two planar hypercoordinate motif 2D materials, namely t-FeC and o-FeC, which are energetically more favorable compared with the reported square and honeycomb lattices. For the t-FeC monolayer, each C atom is quasi-plane four-coordinated with four ambient Fe atoms, considered as the quasi-planar tetragonal lattice, which can provide lower Li adsorption energy, faster Li mobility, and higher theoretical capacity than graphite and MoS_2. In the o-FeC monolayer, each C atom binds to four Fe atoms and one C atom to form a perfect planar pentacoordinate moiety. This monolayer is the first example of a simultaneously pentacoordinate carbon and planar seven-coordinate Fe-containing material.

METHOD

Candidate structures were obtained by using a particle swarm optimization (PSO) method, as implemented in the CALYPSO code;[23−25] it has been successfully applied to various crystal surfaces and low-dimensional materials.[26−28] The vacuum space of 18 Å in the nonperiodic direction was used to minimize the interaction between the neighboring layers. The subsequent structural relaxation and total energy calculations were performed in the Vienna *ab initio* simulation package (VASP).[29] The electron exchange-correlation functional was treated by the Perdew−Burke−Ernzerhof functional within the generalized gradient approximation (GGA) scheme.[30] The energy cutoff of the plane wave was set to 650 eV with an energy precision of 10^{-5} eV.[31] The atomic positions were fully relaxed until the maximum force on each atom was less than 10^{-3} eV per Å. The Brillouin zone was sampled with a 12 × 12 × 1 (12 × 18 × 1 for o-FeC monolayer) Monkhorst−Pack *k*-points grid for static calculations. To account for the strong correlation of an unfilled d orbital of a Fe atom, we also apply the screened hybrid Heyd−Scuseria−Ernzerhof (HSE06) functional[32] and GGA+*U* scheme.[33] We performed band structure calculations with an effective *U* value of 5 eV, in keeping with previous studies.[34,35] Phonon dispersions and frequency densities of states (DOS) were performed in the Phonopy package[36] interfaced with the density functional perturbation theory (DFPT)[37] as performed in VASP. The finite temperature *ab initio* molecular dynamics (AIMD) simulations were performed to further examine the stability of the structure by using time steps of 1 fs in 3 × 3 (2 × 3 for o-FeC monolayer) supercells. The DFT-D2 method of the Grimme van der Waals correction[38] was also used to account for the long-range interactions. The diffusion energy barrier and minimum-energy pathway of Li diffusion on the t-FeC monolayer was calculated by using the nudged elastic band method.[39] More details on computational methods can be found in the Supporting Information.

RESULTS AND DISCUSSION

Configurations and Stabilities. The ground-state structures of Fe−C compounds with 1:1 stoichiometry were selected through a comprehensive PSO search.[23] After extensive structural searching, two low-energy structures were found, labeled as tetragonal-FeC (t-FeC) and orthorhombic-FeC (o-FeC), which are energetically favorable compared with the previously reported square and honeycomb lattices[21,22] (up to 1.18 eV per formula, as listed in Table S1). As shown in Figure 1a, it is observed that fully relaxed t-FeC monolayer

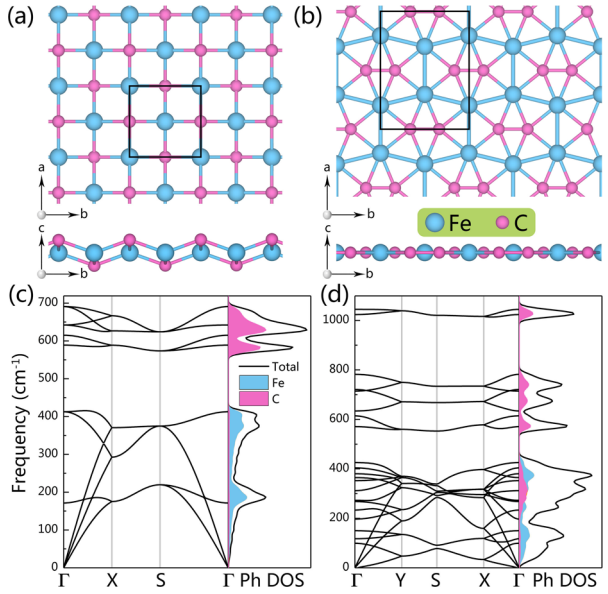

Figure 1. Top and side views of the proposed (a) t-FeC and (b) o-FeC monolayers, respectively. The green lines denote the unit cell; *a* and *b* represent the lattice vectors; the orange and magenta spheres refer to Fe and C atoms, respectively. Calculated phonon dispersion curves of (c) t-FeC and (d) o-FeC monolayers.

crystallizes in a tetragonal lattice with space group *P*4/*nmm*. This t-FeC sheet shows a puckered square structure with a thickness *l* = 1.26 Å. The tetragonal lattice (*a* = *b* = 3.49 Å) is analogous to previously proposed 2D t-TiC,[40] t-YN,[41] t-SiC,[27] rectangular TiN,[42] and rectangular NbN.[43] Figure 1b presents the optimized structure of the o-FeC monolayer. One unit cell of o-FeC monolayer consists of four Fe and C atoms, with the optimized lattice constants of *a* = 5.96 Å and *b* = 4.49 Å, respectively. The length of the Fe−C bond in this monolayer (1.85 Å) is noticeably smaller than that in the bulk FeC_2 sheet (1.84−2.11 Å), indicating a much stronger interaction between the Fe and C atoms. Additionally, we also considered the buckled structure of o-FeC monolayer and found that the planar structure is lower in energy than the buckled structure.

Therefore, unlike the t-FeC monolayer with puckered structure, o-FeC monolayer shows a perfect planar lattice with space group *Cmmm*. In this planar sheet, each C atom coordinates with five adjacent atoms (one C atom and four Fe atoms), thus forming planar pentacoordinate moiety, while each Fe atom coordinates with four carbon atoms and three Fe atoms, forming a planar seven-coordinate moiety. The optimized Fe−C bond length (1.91−1.94 Å) is about the same as that in the FeC_2 sheet (1.84−2.11 Å),[35] but slightly larger than that in the t-FeC monolayer (1.86 Å), while we notice that the bond length of Fe−Fe is 2.31−2.44 Å, which is close to the previous result of 2.33 Å in the square iron membranes.[21,44]

To assess the energetic stability of the proposed structures, we first compare the relative energies of t-FeC and o-FeC structures with previously reported structures, namely, square-FeC and honeycomb-FeC.[21] As shown in Table S1 and Figure S1, all functionals prefer t-FeC and o-FeC significantly compared with previously reported planar honeycomb and

https://dx.doi.org/10.1021/acsami.0c03764
ACS Appl. Mater. Interfaces 2020, 12, 30297−30303

square lattices.[21] We then calculated the cohesive energy to further check the stability of proposed structures, which is defined as $E_{coh} = (nE_{Fe} + mE_C - E_{Total})/(n + m)$, in which E_{Fe}, E_C, and E_{Total} are the total energies of a single Fe atom, a single C atom, and proposed monolayers, respectively; n and m are the numbers of Fe and C atoms in the unit cell, respectively. The calculated cohesive energies of t-FeC and o-FeC are 5.76 and 5.59 eV per atom, respectively, which are higher than those of Be_5C_2 (4.58 eV per atom),[45] Be_2C (4.86 eV per atom),[16] FeB_2 (4.87 eV per atom),[46] and Cu_2Si monolayer (3.46 eV per atom)[18] at the same theoretical level. Therefore, the even higher cohesive energy can ensure that t-FeC and o-FeC monolayers are strongly connected networks.

The stability of t-FeC and o-FeC monolayers was further investigated by calculating the phonon dispersion curves and phonon density of states (Ph DOS) along the high-symmetry directions. As shown in Figures 1c and 1d, there is no sign of an imaginary phonon frequency observed in the entire Brillouin zone. Simultaneously, the calculated Ph DOS also reveals that there is no phonon with imaginary frequency in these monolayers, which very well agree with the phonon dispersion curves. The results demonstrate that these two monolayers are dynamically stable. In particular, for o-FeC, the highest frequency of optical modes reaches around 1047 cm^{-1}, which is much higher than the highest frequency of 854 cm^{-1} in FeB_2,[46] 580 cm^{-1} in silicene,[47] and 420 cm^{-1} in Cu_2Si monolayer,[18] suggesting a robust Fe−C interaction. Therefore, although the calculated relative energy of o-FeC is higher than that of t-FeC by 0.34 eV per formula, the former still represents a strongly bonded network.

Moreover, to verify that the proposed new materials will be stable at ambient temperatures, we performed AIMD simulations using a 3 × 3 supercell for t-FeC and a 2 × 3 supercell for o-FeC monolayers at different temperatures of 500, 1500, and 2000 K with a time step of 1 fs, as shown in Figure S2. After AIMD simulation of 5 ps, snapshots taken at the end of each simulation time are illustrated in Figure S3. From the snapshots, all proposed monolayers can maintain its structural integrity at 2000 K. The above results reveal that the monolayers exhibit very high thermal stability and can maintain its structural integrity up to 2000 K. It is worth noting that we also tested the 10 ps simulation using a larger 5 × 5 supercell for the t-FeC monolayer and finally found that the structure is still stable, as shown in Figure S4.

The mechanical properties are another important parameters for the potential applications of 2D materials. Generally, the in-plane stiffness (or in-plane Young modulus) is used to assess the mechanical stability of 2D materials. As listed in Table S2, we compare the calculated value of the t-FeC and o-FeC sheets to previous experimental or theoretical values of several 2D materials, including graphene, borophone, and B_2C sheets.[15,48] For the t-FeC monolayer, the in-plane stiffness was computed to be 77 N m^{-1}, which is lower than that of graphene. However, it is comparable to the in-plane stiffness of the Cu_2Si monolayer (93 N m^{-1}), and higher than germanene (42 N m^{-1}), suggesting that monolayers have good mechanical properties. For the o-FeC monolayer, the calculated in-plane stiffness is 203 N m^{-1} (along the a-direction) and 218 N m^{-1} (along the b-direction). As these values are not equal to each other, the o-FeC monolayer is mechanically anisotropic, and the in-plane stiffness of o-FeC is obviously higher than t-FeC. Thus, the proposed monolayers show strong mechanical stability.

Unusual Chemical Bonding Features. In view of the unique bonding features in the monolayers, we then analyze the electron localization function (ELF) and deformation electron density (DED) to better understand the bonding features of these monolayers. The ELF analysis is a useful strategy for identifying and visualizing electron localization in molecules or solids.[49] The values are renormalized between 0.00 and 1.00, and in general, the values of 1.00 and 0.50 represent the fully localized and fully delocalized of the electrons, respectively, while the nearer the values are to zero, the lower the charge density is.[50] As shown in Figure 2, the t-

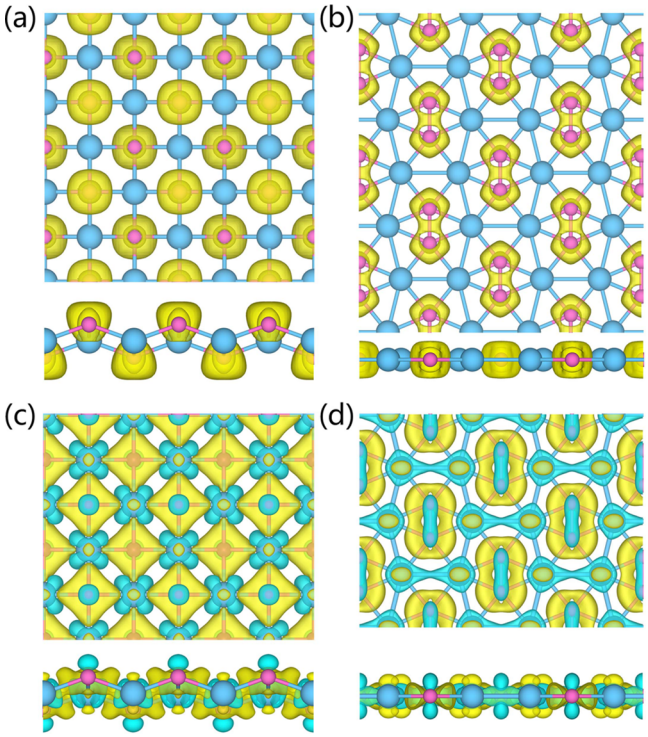

Figure 2. Isosurfaces of ELF with the value of 0.70 for (a) t-FeC and (b) o-FeC. Deformation charge density of (c) t-FeC and (d) o-FeC monolayer. Green and blue refer to electron accumulation and depletion regions. The isovalue is 0.01e/Å^3.

FeC monolayer exhibits a clearly ELF image: the ptC containing Fe−C network, where ELF distributes around the C-centered four Fe−C bonds. In the t-FeC monolayer, the DED map reveals that electron transfers from the Fe to C atom as shown in Figure 2c, and Bader analysis shows a charge transfer of 0.77e from each Fe atom. The transferred electrons, particularly from the Fe-d state, are delocalized around the four Fe−C bonds. Simultaneously, the C-p state is found to partially deplete and delocalize over the four Fe−C bonds. Therefore, the delocalized electron states in t-FeC monolayer not only recede the atomic activity in forming out-of-plane bonds but also strengthen the in-plane Fe−C bonds, which is crucial for stabilizing this planar four-coordinate moiety.[27,40]

Interestingly, the o-FeC monolayer exhibits a dumbbell-like ELF image, which is featured by two C atoms surrounded by adjacent Fe atoms. In this novel ELF maps, one part is distributed around the Fe−C bonds, where ELF distributes around the C-centered Fe−C bonds, while another part is the C−C dimer structure. Therefore, o-FeC contains one C−C σ bond and four Fe−C bonds for one C atom. Bader analysis

https://dx.doi.org/10.1021/acsami.0c03764
ACS Appl. Mater. Interfaces 2020, 12, 30297−30303

shows a charge transfer of 0.69*e* from each Fe atom, and each C atom captures ≈0.65*e* from Fe atoms. Moreover, as shown in Figure 2d, a significant electron transfer from Fe to C atoms, as identified by the different colored regions in the DED map, results in the electronic supplement for monolayer and thus stabilizes this pure planar framework. This significant electron transfer agrees with the larger electronegativity of carbon (2.55) than iron (1.83).

Electronic Properties. To identify the magnetic ground states of t-FeC and o-FeC, various magnetic orders, including nonmagnetic (NM), ferromagnetic (FM), and antiferromagnetic (AFM) ordering, are considered. As listed in Table S3, t-FeC possesses NM ordering, whereas FM coupling is preferred over the NM state for o-FeC (Figure S5). The calculated DOS indicates that the magnetism in o-FeC monolayer is mainly contributed by the d orbitals of Fe atoms (Figure S6). We also recalculated their band structures by using the HSE06 scheme (the PBE and GGA+*U* results are shown in Figure S7), shown in Figure S8. The metallic characters of sheets are demonstrated by the Fermi level being located inside the bands, and no apparent band gap around the Fermi level is observed. As expected, the strongest contributions at the Fermi level originate from the Fe-d and C-p states. For t-FeC, it is noteworthy that the high peaks of DOS appear around the Fermi level, suggesting the high density of carriers at the Fermi level. These high densities of electron states suggest that the electrons can efficiently participate in the electronic transport process, leading to the outstanding electron conductivity of the t-FeC monolayer. The accompanying electric conductivity is in accordance with the delocalized electrons as investigated by ELF and DED analysis.

Performance in Li-Ion Batteries. As mentioned in the aforementioned section, the intrinsic metallicity of the global minimum t-FeC monolayer makes it a potential anode material in Li-ion batteries. Therefore, we investigated the adsorption energy and diffusion of Li-ion on the t-FeC monolayer. We first collected some high-symmetry adsorption sites and then deposited a single Li atom on each adsorption site of a 3 × 3 supercell. As shown in Figure S9, the most favorable Li adsorption position located on the top of the C atoms, and the adsorption energy is −1.89 eV per Li atom, suggesting the high stability of the t-FeC−Li complex systems. Two possible diffusion pathways are investigated in a 3 × 3 supercell as shown in Figure 3. When Li moves through the pathway 1, only a small energy barrier of 0.26 eV should be overcome, which is close to that of MoS_2 (0.25) and commercially used graphite anode (0.22 eV).[51] With the increase of Li-ion concentration, as shown in Figure 3c, the Li adsorption energy of t-FeCLi_x decreases gradually with the increase of *x* because more pronounced repulsive Coulomb interactions exist between neighboring Li atoms with smaller distance.[52] Surprisingly, t-FeCLi_x can provide a Li adsorption energy of −0.38 eV per Li atom even at *x* = 4, indicating that Li atoms can be stably adsorbed on monolayer at such a high concentration (adsorption structures are shown in Figure S10). Therefore, when the t-FeC monolayer reaches the highest Li storage capacity, *x* = 4 (t-FeCLi_4), the estimated open-circuit voltage (OCV) is 0.37 V, and the theoretical capacity is calculated to be 1579 mAh g^{-1}, which is distinctly higher than that of commercialized graphite (C_6Li, 372 mAh g^{-1}), demonstrating t-FeC is a promising candidate anode for Li-ion batteries.

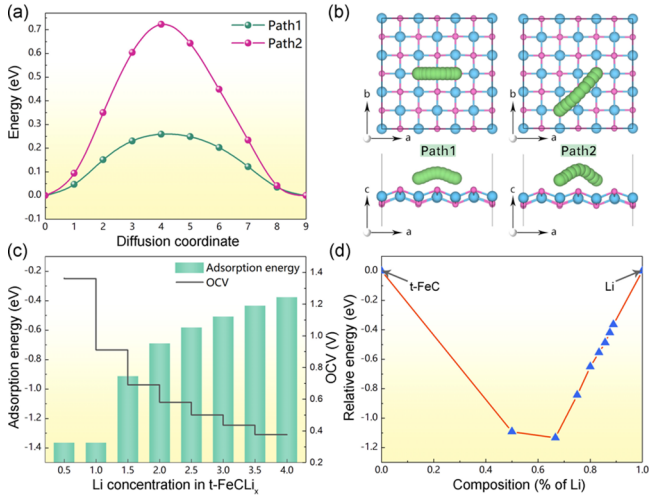

Figure 3. (a) Lithium diffusion pathway on the surface of t-FeC monolayer. (b) Corresponding diffusion barrier profiles of Li on t-FeC monolayer through the predesigned pathways (paths 1 and 2). (c) Variation of adsorption energy and calculated voltage profile as a function of Li concentration in t-FeCLi_x. (d) Relative stabilities of t-FeCLi_x (the *x* value from 0.5 to 4 corresponds to eight stable adsorption structures) with respect to bulk Li and t-FeC sheet at 0 K. The red line connecting shows the convex hull. The adsorption configurations located on the convex hull are thermodynamically stable against decomposition into other phases.

To further compare the formation energy of t-FeC-Li_x compounds with different compositions, the relative energy is calculated. The results are presented in the form of the convex hull in Figure 3d, which denotes the static stability of t-FeC−Li_x compounds at 0 K. Generally, the complex systems located on the convex hull are thermodynamically stable against decomposition into other phases.[53,54] According to this criterion, all considered adsorption structures are thermodynamically stable. Meanwhile, all considered adsorption structures are metallic during the Li-ion intercalation process (see Figures S11 and S12), suggesting the good electrical conductivity in the charge/discharge cycle process. We also performed AIMD simulations (4 × 4 supercell containing 198 atoms) at the temperature of 300 K to investigate the stability of the t-FeCLi_4 adsorption configuration. During the AIMD simulation (up to 10 ps) process, the total energy of t-FeCLi_4 reaches equilibrium promptly and then uctuates near the equilibrium state (see Figure 4a). Particularly, t-FeC lattice in the t-FeCLi_4 supercell can maintain the structural integrity during the whole simulation process, suggesting the t-FeC monolayer has good stability in the lithiation process.

As mentioned above, we have demonstrated that our predicted t-FeC monolayer shows great advantage in Li-ion storage and diffusion, especially for its ultrahigh Li-ion specific capacity (up to 1579 mAh g^{-1}) in comparison to the well-studied Ti_3C_2 or Ti_2C (320−440 mAh g^{-1}).[55−57] As a comparison, Ti_3C_2 or Ti_2C sheets need surface functionalization,[58,59] which will distinctly reduce both specific capacity and cycle life. However, the t-FeC monolayer can adsorb Li atoms directly without any surface functionalization. The high specific capacity of the t-FeC monolayer can also be understood by the unique tetragonal lattice which contains both sufficient adsorption sites and adsorbent area for Li atom. Simultaneously, the delocalized electronic distribution also plays a vital role in the stabilization of multilayer Li absorption and storage.

https://dx.doi.org/10.1021/acsami.0c03764
ACS Appl. Mater. Interfaces 2020, 12, 30297−30303

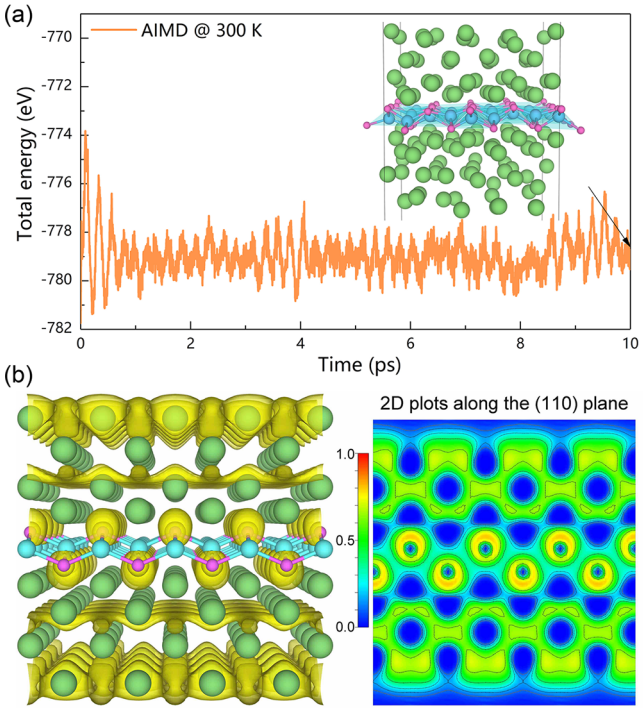

Figure 4. (a) Fluctuation of the total energy of t-FeCLi$_4$ adsorption configuration during the AIMD simulation step with 10 ps at 300 K. Snapshot of the t-FeCLi$_4$ structures at the end of 10 ps AIMD simulation is also presented. (b) Calculated ELF of pristine t-FeC monolayer with four-layer Li atoms (left). The corresponding 2D ELF map showing at (110) cutoff plane is also plotted (right).

It is apparent from Figure 4b and Figure S13 that more electrons transfer from the inner layer to the outer layer (compared with t-FeCLi and t-FeCLi$_3$ systems) and mainly distribute among the outer-layer Li ions, resulting in the high adsorption capacity of the t-FeC monolayer.

CONCLUSION

To summarize, by means of systematic *ab initio* computations, the energetically stable 2D Fe−C allotropes featured by planar hypercoordinate chemical bonding are proposed. In the t-FeC monolayer, each C atom bonds to four Fe atoms to form a quasi-phC moiety. The predicted monolayers in this work are the absence of imaginary phonon modes and can be stable up to 2000 K in the AIMD simulations, indicating a great potential to be realized experimentally. The calculated low adsorption energy, high theoretical capacity, and small diffusion barrier indicate that t-FeC is a promising candidate for Li-ion batteries.

ASSOCIATED CONTENT

Supporting Information

The Supporting Information is available free of charge at https://pubs.acs.org/doi/10.1021/acsami.0c03764.

Details of lattice parameters, elastic constants, in-plane Young's modulus and Poisson's ratio of t-FeC and o-FeC, details of structure of honeycomb-FeC and square-FeC monolayers, details of band structure for t-FeC and o-FeC at the GGA+*U* level (PDF)

AUTHOR INFORMATION

Corresponding Author

Xiaojun Hu − *College of Materials Science and Engineering, Zhejiang University of Technology, Hangzhou 310014, China;* orcid.org/0000-0001-7851-9900; Email: huxj@zjut.edu.cn

Authors

Dong Fan − *College of Materials Science and Engineering, Zhejiang University of Technology, Hangzhou 310014, China;* orcid.org/0000-0003-1873-3416

Chengke Chen − *College of Materials Science and Engineering, Zhejiang University of Technology, Hangzhou 310014, China*

Shaohua Lu − *College of Materials Science and Engineering, Zhejiang University of Technology, Hangzhou 310014, China*

Xiao Li − *College of Materials Science and Engineering, Zhejiang University of Technology, Hangzhou 310014, China*

Meiyan Jiang − *College of Materials Science and Engineering, Zhejiang University of Technology, Hangzhou 310014, China*

Complete contact information is available at: https://pubs.acs.org/10.1021/acsami.0c03764

Author Contributions

X.H. and D.F. designed the research. D.F. performed the systematic structure search and *ab initio* calculations and interpreted the data. D.F. wrote the manuscript with the support from S.L., C.C., X.L., and M.J. X.H. coordinated the research.

Notes

The authors declare no competing financial interest.

The structural (vasp) data in this work, and the output of aNVT-MD simulation results, that support the findings of this study are available at https://github.com/agrh/Papers. Any other information supporting the conclusions presented is available from the authors upon request.

ACKNOWLEDGMENTS

This work was performed at the National Supercomputer Center in Guangzhou, and the calculations were performed on TianHe-2. This work was supported by the Key Project of National Natural Science Foundation of China (U1809210), the National Natural Science Foundation of China (Grants 11504325, 50972129, and 50602039), and the Natural Science Foundation of Zhejiang Province (LQ15A040004). This work was also supported by the National Key Research and Development Program of China (No. 2016YFE0133200), the European Union's Horizon 2020 Research and Innovation Staff Exchange (RISE) Scheme (No. 734578), and the One Belt and One Road International Cooperation Project from Key Research and Development Program of Zhejiang Province (2018C04021).

REFERENCES

(1) Yang, L.-M.; Ganz, E.; Chen, Z.; Wang, Z.-X.; Schleyer, P. v. R. Four Decades of the Chemistry of Planar Hypercoordinate Compounds. *Angew. Chem., Int. Ed.* **2015**, *54*, 9468−9501.

(2) Wang, Y.; Li, Y.; Chen, Z. Planar Hypercoordinate Motifs in Two-Dimensional Materials. *Acc. Chem. Res.* **2020**, *53*, 887−895.

(3) Nair, R. R.; Blake, P.; Grigorenko, A. N.; Novoselov, K. S.; Booth, T. J.; Stauber, T.; Peres, N. M.; Geim, A. K. Fine Structure Constant Defines Visual Transparency of Graphene. *Science* **2008**, *320*, 1308−1308.

(4) Smith, P.; Buseck, P. R. Carbyne Forms of Carbon: Do They Exist? *Science* **1982**, *216*, 984−986.

(5) Hoffmann, R.; Alder, R. W.; Wilcox, C. F., Jr. Planar Tetracoordinate Carbon. *J. Am. Chem. Soc.* **1970**, *92*, 4992−4993.
(6) Cotton, F. A.; Millar, M. The Probable Existence of a Triple Bond Between Two Vanadium Atoms. *J. Am. Chem. Soc.* **1977**, *99*, 7886−7891.
(7) Harder, S.; Boersma, J.; Brandsma, L.; Van Heteren, A.; Kanters, J. A.; Bauer, W.; Schleyer, P. v. R. Planar Tetracoordinate Carbon Atoms Hidden in the Tetrameric Aggregate of (2,6-Dimethoxyphenyl) Lithium. *J. Am. Chem. Soc.* **1988**, *110*, 7802−7806.
(8) Wang, Z.-X.; Schleyer, P. v. R. The Theoretical Design of Neutral Planar Tetracoordinate Carbon Molecules with $C(C)_4$ Substructures. *J. Am. Chem. Soc.* **2002**, *124*, 11979−11982.
(9) Li, X.; Wang, L.-S.; Boldyrev, A. I.; Simons, J. Tetracoordinated Planar Carbon in the Al_4C-anion. A Combined Photoelectron Spectroscopy and Ab Initio Study. *J. Am. Chem. Soc.* **1999**, *121*, 6033−6038.
(10) Sun, W.; Zhang, C.; Cao, Z. Novel Beltlike and Tubular Structures of Boron and Carbon Clusters Containing the Planar Tetracoordinate Carbon: A Theoretical Study of $(C_3B_2)_nH_4$ (n = 2−6) and $(C_3B_2)_n$ (n = 4−8). *J. Phys. Chem. C* **2008**, *112*, 351−357.
(11) Minyaev, R.; Avakyan, V.; Starikov, A.; Gribanova, T.; Minkin, V. Extended Organoboron Structures Containing Several Planar Tetracoordinate Carbon Atoms. *Dokl. Chem.* **2008**, *419*, 101−107.
(12) Wang, Z.-X.; von Ragué Schleyer, P. Construction Principles of " Hyparenes": Families of Molecules with Planar Pentacoordinate Carbons. *Science* **2001**, *292*, 2465−2469.
(13) Erhardt, S.; Frenking, G.; Chen, Z.; Schleyer, P. v. R. Aromatic Boron Wheels with More Than One Carbon Atom in ihe Center: C_2B_8, $C_3B_9^{3+}$, and $C_5B_{11}^{+}$. *Angew. Chem., Int. Ed.* **2005**, *44*, 1078−1082.
(14) Ito, K.; Chen, Z.; Corminboeuf, C.; Wannere, C. S.; Zhang, X. H.; Li, Q. S.; Schleyer, P. v. R. Myriad Planar Hexacoordinate Carbon Molecules Inviting Synthesis. *J. Am. Chem. Soc.* **2007**, *129*, 1510−1511.
(15) Wu, X.; Pei, Y.; Zeng, X. C. B_2C Graphene, Nanotubes, And Nanoribbons. *Nano Lett.* **2009**, *9*, 1577−1582.
(16) Li, Y.; Liao, Y.; Chen, Z. Be_2C Monolayer with Quasi-Planar Hexacoordinate Carbons: A Global Minimum Structure. *Angew. Chem., Int. Ed.* **2014**, *53*, 7248−7252.
(17) Zhu, C.; Lv, H.; Qu, X.; Zhang, M.; Wang, J.; Wen, S.; Li, Q.; Geng, Y.; Su, Z.; Wu, X.; Li, Y.; Ma, Y. TMC(TM = Co, Ni, and Cu) Monolayers with Planar Pentacoordinate Carbon and Their Potential applications. *J. Mater. Chem. C* **2019**, *7*, 6406−6413.
(18) Yang, L.-M.; Bacic, V.; Popov, I. A.; Boldyrev, A. I.; Heine, T.; Frauenheim, T.; Ganz, E. Two-dimensional Cu_2Si Monolayer with Planar Hexacoordinate Copper and Silicon Bonding. *J. Am. Chem. Soc.* **2015**, *137*, 2757−2762.
(19) Feng, B.; Fu, B.; Kasamatsu, S.; Ito, S.; Cheng, P.; Liu, C.-C.; Feng, Y.; Wu, S.; Mahatha, S. K.; Sheverdyaeva, P.; et al. Experimental Realization of Two-dimensional Dirac Nodal Line Fermions in Monolayer Cu_2Si. *Nat. Commun.* **2017**, *8*, 1007.
(20) Zhao, J.; Deng, Q.; Bachmatiuk, A.; Sandeep, G.; Popov, A.; Eckert, J.; Rümmeli, M. H. Free-standing Single-atom-thick Iron Membranes Suspended in Graphene Pores. *Science* **2014**, *343*, 1228−1232.
(21) Thomsen, M. R.; Brun, S. J.; Pedersen, T. G. Stability and Magnetization of Free-standing and Graphene-embedded Iron Membranes. *Phys. Rev. B: Condens. Matter Mater. Phys.* **2015**, *91*, 125439.
(22) Shao, Y.; Pang, R.; Shi, X. Stability of Two-dimensional Iron Carbides Suspended Across Graphene Pores: First-principles Particle Swarm Optimization. *J. Phys. Chem. C* **2015**, *119*, 22954−22960.
(23) Wang, Y.; Lv, J.; Zhu, L.; Ma, Y. Crystal Structure Prediction via Particle-swarm Optimization. *Phys. Rev. B: Condens. Matter Mater. Phys.* **2010**, *82*, 094116.
(24) Gao, P.; Tong, Q.; Lv, J.; Wang, Y.; Ma, Y. X-ray Diffraction Data-assisted Structure Searches. *Comput. Phys. Commun.* **2017**, *213*, 40−45.
(25) Gao, B.; Gao, P.; Lu, S.; Lv, J.; Wang, Y.; Ma, Y. Interface Structure Prediction via CALYPSO Method. *Sci. Bull.* **2019**, *64*, 301−309.
(26) Lu, S.; Wang, Y.; Liu, H.; Miao, M.-s.; Ma, Y. Self-assembled Ultrathin Nanotubes on Diamond (100) Surface. *Nat. Commun.* **2014**, *5*, 3666.
(27) Fan, D.; Lu, S.; Guo, Y.; Hu, X. Novel Bonding Patterns and Optoelectronic Properties of the Two-dimensional Si_xC_y Monolayers. *J. Mater. Chem. C* **2017**, *5*, 3561−3567.
(28) Fan, D.; Lu, S.; Guo, Y.; Hu, X. Two-dimensional Stoichiometric Boron Carbides with Unexpected Chemical Bonding and Promising Electronic Properties. *J. Mater. Chem. C* **2018**, *6*, 1651−1658.
(29) Kresse, G.; Furthmüller, J. Efficient Iterative Schemes for Ab Initio Total-energy Calculations Using a Plane-wave Basis Set. *Phys. Rev. B: Condens. Matter Mater. Phys.* **1996**, *54*, 11169.
(30) Perdew, J. P.; Burke, K.; Ernzerhof, M. Generalized Gradient Approximation Made Simple. *Phys. Rev. Lett.* **1996**, *77*, 3865.
(31) Fan, D.; Lu, S.; Golov, A. A.; Kabanov, A. A.; Hu, X. D-carbon: Ab initio study of a novel carbon allotrope. *J. Chem. Phys.* **2018**, *149*, 114702.
(32) Heyd, J.; Scuseria, G. E.; Ernzerhof, M. Hybrid Functionals Based on a Screened Coulomb Potential. *J. Chem. Phys.* **2003**, *118*, 8207−8215.
(33) Dudarev, S.; Botton, G.; Savrasov, S.; Humphreys, C.; Sutton, A. Electron-energy-loss Spectra and the Structural Stability of Nickel Oxide: An LSDA+U study. *Phys. Rev. B: Condens. Matter Mater. Phys.* **1998**, *57*, 1505.
(34) Anisimov, V.; Elfimov, I.; Hamada, N.; Terakura, K. Charge-ordered Insulating State of Fe_3O_4 from First-principles Electronic Structure Calculations. *Phys. Rev. B: Condens. Matter Mater. Phys.* **1996**, *54*, 4387.
(35) Zhao, T.; Zhou, J.; Wang, Q.; Kawazoe, Y.; Jena, P. Ferromagnetic and Half-Metallic FeC_2 Monolayer Containing C_2 Dimers. *ACS Appl. Mater. Interfaces* **2016**, *8*, 26207−26212.
(36) Togo, A.; Tanaka, I. First Principles Phonon Calculations in Materials Science. *Scr. Mater.* **2015**, *108*, 1−5.
(37) Baroni, S.; De Gironcoli, S.; Dal Corso, A.; Giannozzi, P. Phonons and Related Crystal Properties from Density-functional Perturbation Theory. *Rev. Mod. Phys.* **2001**, *73*, 515.
(38) Grimme, S. Semiempirical GGA-type Density Functional Constructed with a Long-range Dispersion Correction. *J. Comput. Chem.* **2006**, *27*, 1787−1799.
(39) Henkelman, G.; Uberuaga, B. P.; Jónsson, H. A Climbing Image Nudged Elastic Band Method for Finding Saddle Points and Minimum Energy Paths. *J. Chem. Phys.* **2000**, *113*, 9901−9904.
(40) Zhang, Z.; Liu, X.; Yakobson, B. I.; Guo, W. Two-dimensional Tetragonal TiC Monolayer Sheet and Nanoribbons. *J. Am. Chem. Soc.* **2012**, *134*, 19326−19329.
(41) Xu, B.; Xiang, H.; Yin, J.; Xia, Y.; Liu, Z. A Two-dimensional Tetragonal Yttrium Nitride Monolayer: A Ferroelastic Semiconductor with Switchable Anisotropic Properties. *Nanoscale* **2018**, *10*, 215−221.
(42) Zhou, L.; Zhuo, Z.; Kou, L.; Du, A.; Tretiak, S. Computational Dissection of Two-Dimensional Rectangular Titanium Mononitride TiN: Auxetics and Promises for Photocatalysis. *Nano Lett.* **2017**, *17*, 4466−4472.
(43) Anand, S.; Thekkepat, K.; Waghmare, U. V. Two-Dimensional Rectangular and Honeycomb Lattices of NbN: Emergence of Piezoelectric and Photocatalytic Properties at Nanoscale. *Nano Lett.* **2016**, *16*, 126−131.
(44) Nevalaita, J.; Koskinen, P. Atlas for the Properties of Elemental Two-dimensional Metals. *Phys. Rev. B: Condens. Matter Mater. Phys.* **2018**, *97*, 035411.
(45) Wang, Y.; Li, F.; Li, Y.; Chen, Z. Semi-metallic Be_5C_2 Monolayer Global Minimum with Quasi-planar Pentacoordinate Carbons and Negative Poisson's Ratio. *Nat. Commun.* **2016**, *7*, 11488.

https://dx.doi.org/10.1021/acsami.0c03764
ACS Appl. Mater. Interfaces 2020, 12, 30297−30303

(46) Zhang, H.; Li, Y.; Hou, J.; Du, A.; Chen, Z. Dirac State in the FeB_2 Monolayer with Graphene-like Boron Sheet. *Nano Lett.* **2016**, *16*, 6124−6129.
(47) Cahangirov, S.; Topsakal, M.; Aktürk, E.; Şahin, H.; Ciraci, S. Two- and One-dimensional Honeycomb Structures of Silicon and Germanium. *Phys. Rev. Lett.* **2009**, *102*, 236804.
(48) Mannix, A. J.; Zhou, X.-F.; Kiraly, B.; Wood, J. D.; Alducin, D.; Myers, B. D.; Liu, X.; Fisher, B. L.; Santiago, U.; Guest, J. R.; Yacaman, M. J.; Ponce, A.; Oganov, A. R.; Hersam, M. C.; Guisinger, N. P. Synthesis of Borophenes: Anisotropic, Two-dimensional Boron Polymorphs. *Science* **2015**, *350*, 1513−1516.
(49) Savin, A.; Nesper, R.; Wengert, S.; Fässler, T. F. ELF: The Electron Localization Function. *Angew. Chem., Int. Ed. Engl.* **1997**, *36*, 1808−1832.
(50) Savin, A.; Jepsen, O.; Flad, J.; Andersen, O. K.; Preuss, H.; von Schnering, H. G. Electron Localization in Solid-state Structures of the Elements: The Diamond Structure. *Angew. Chem., Int. Ed. Engl.* **1992**, *31*, 187−188.
(51) Jing, Y.; Zhou, Z.; Cabrera, C. R.; Chen, Z. Metallic VS_2 Monolayer: A Promising 2D Anode Material for Lithium Ion Batteries. *J. Phys. Chem. C* **2013**, *117*, 25409−25413.
(52) Fan, D.; Lu, S.; Guo, Y.-D.; Hu, X. Two-Dimensional Tetragonal Titanium Carbide: A High-Capacity and High-Rate Battery Material. *J. Phys. Chem. C* **2018**, *122*, 15118−15124.
(53) Zhu, L.; Liu, H.; Pickard, C. J.; Zou, G.; Ma, Y. Reactions of Xenon with Iron and Nickel Are Predicted in the Earthas Inner Core. *Nat. Chem.* **2014**, *6*, 644.
(54) Yu, T.; Zhao, Z.; Liu, L.; Zhang, S.; Xu, H.; Yang, G. TiC_3 Monolayer with High Specific Capacity for Sodium-ion Batteries. *J. Am. Chem. Soc.* **2018**, *140*, 5962−5968.
(55) Tang, Q.; Zhou, Z.; Shen, P. Are MXenes Promising Anode Materials for Li Ion Batteries? Computational Studies on Electronic Properties and Li Storage Capability of Ti_3C_2 and $Ti_3C_2X_2$ (X = F, OH) Monolayer. *J. Am. Chem. Soc.* **2012**, *134*, 16909−16916.
(56) Anasori, B.; Lukatskaya, M. R.; Gogotsi, Y. 2D Metal Carbides and Nitrides (MXenes) for Energy Storage. *Nat. Rev. Mater.* **2017**, *2*, 16098.
(57) Naguib, M.; Mochalin, V. N.; Barsoum, M. W.; Gogotsi, Y. 25th Anniversary Article: MXenes: A New Family of Two-dimensional Materials. *Adv. Mater.* **2014**, *26*, 992−1005.
(58) Xie, Y.; Naguib, M.; Mochalin, V. N.; Barsoum, M. W.; Gogotsi, Y.; Yu, X.; Nam, K.-W.; Yang, X.-Q.; Kolesnikov, A. I.; Kent, P. R. Role of Surface Structure on Li-ion Energy Storage Capacity of Two-dimensional Transition-metal Carbides. *J. Am. Chem. Soc.* **2014**, *136*, 6385−6394.
(59) Naguib, M.; Halim, J.; Lu, J.; Cook, K. M.; Hultman, L.; Gogotsi, Y.; Barsoum, M. W. New Two-dimensional Niobium and Vanadium Carbides as Promising Materials for Li-ion Batteries. *J. Am. Chem. Soc.* **2013**, *135*, 15966−15969.

https://dx.doi.org/10.1021/acsami.0c03764
ACS Appl. Mater. Interfaces 2020, 12, 30297−30303